AGU PUBLICATIONS

JGR

Journal of Geophysical Research: Space Physics

RESEARCH ARTICLE

10.1002/2013JA019590

Two-dimensional hybrid models of H^+-He^{++} expanding solar wind plasma heating

L. Ofman[1,2], A. F. Viñas[3], and Y. Maneva[1,4]

[1]CUA and NASA/GSFC, Greenbelt, Maryland, USA, [2]Department of Geophysics, Tel Aviv University, Ramat Aviv, Israel, [3]NASA/GSFC, Greenbelt, Maryland, USA, [4]Now at CmPA/KU Leuven, Celestijnenlaan 200B, Leuven, Belgium

Key Points:
- Heating of the solar wind ions by waves is studied with the hybrid model
- The effects of expansion on anisotropic solar wind ion heating are studied
- Drift instability can heat the solar wind ions consistent with observations

Supporting Information:
- Readme
- Movie S1

Correspondence to:
L. Ofman,
Leon.Ofman@nasa.gov

Citation:
Ofman, L., A. F. Viñas, and Y. Maneva (2014), Two-dimensional hybrid models of H^+-He^{++} expanding solar wind plasma heating, *J. Geophys. Res. Space Physics*, *119*, 4223–4238, doi:10.1002/2013JA019590.

Received 1 NOV 2013
Accepted 29 MAY 2014
Accepted article online 6 JUN 2014
Published online 26 JUN 2014

Abstract Preferential heating and acceleration of the solar wind He^{++} ions compared to protons in fast solar wind streams have been known for decades, thanks to in situ spacecraft measurements at 0.29–5 AU. Turbulent magnetic field fluctuations with approximate power law spectra have been observed as well. However, the exact causes of these processes are still not known due to the lack of detailed information on the magnetic field fluctuations and ion velocity distributions in the acceleration region of the solar wind. Here the collisionless heating processes in expanding solar wind plasma are investigated using 2-D hybrid modeling with parameters appropriate to the heliocentric distance of 10 R_S. In this study the ion dynamics is described kinetically, while electrons are treated as a background massless fluid in an expanding solar wind model. The source of free energy for the heating is introduced through an initial nonequilibrium state of the plasma with large He^{++} ion temperature anisotropy or with super-Alfvénic relative ion drift. We also employ an externally imposed spectrum of magnetic fluctuations in the frequency range below the proton gyroresonant frequency to heat the He^{++} ions. We investigate the effects of solar wind radial expansion by modeling several values of the expansion rate in a parametric study. We find that the preferential ion heating is attained in both nonexpanding and expanding solar wind models. Thus, the expansion has little effect on the preferential He^{++} ion heating by the processes considered here. Moreover, the expansion leads to faster evolution of the magnetosonic drift instability, reducing the drift velocity to lower values sooner, and the corresponding generation of the magnetic fluctuations that heat the ions, compared to the nonexpanding case. This is due to the reduction of the perpendicular particle velocities in the expanding (inflated) frame. For cases with little proton perpendicular heating, the solar wind expansion leads to the reduction of the proton temperature anisotropy to values less than one in the low-$\beta_{p\|}$ solar wind acceleration region consistent with some observed values. However, this effect must be offset by perpendicular proton heating—likely by the same process that heats the He^{++} ions to be consistent with the full range of observed proton perpendicular temperature values.

1. Introduction

The heating of the multi-ion solar wind plasma has been intensively studied for decades using satellite observations and theoretical modeling. The important role of waves in this process in the fast solar wind has been demonstrated in many studies (see the review by *Ofman* [2010b]). However, the kinetic details of the heating and the related processes in the non-Maxwellian solar wind plasma are not yet fully understood. In situ measurements of Ulysses and Helios spacecraft in the high-speed solar wind streams have revealed a variety of nonthermal features of ion velocity distributions [e.g., *Marsch*, 1991; *Feldman et al.*, 1996; *Neugebauer et al.*, 1996]. Proton distributions often appeared as double-peaked streams, while the He^{++} ions drift at the local Alfvén speed relative to the protons [e.g., *Marsch et al.*, 1982a, 1982b; *Goldstein et al.*, 2000; *Bourouaine et al.*, 2013]. Recent MErcury Surface, Space Environment, GEochemistry, and Ranging (MESSENGER) observations at ~0.3 AU confirm and extend past observations close to the Sun [*Gershman et al.*, 2012]. The dependence of the proton temperature anisotropy on the parallel proton plasma $\beta_{p\|}$, obtained from ACE/Wind measurements in the fast solar wind, shows parametric dependence with many data points that appear above the threshold for the ion cyclotron instability, and the data seem to be constrained by the theoretical threshold of firehose and mirror instabilities [*Bale et al.*, 2009]. *Maruca et al.* [2011] further expanded this study using Wind data and concluded that heating processes are more effective than cooling processes at creating and maintaining proton temperature anisotropy in the solar wind. The ion temperature anisotropies are strongly affected by the value of the relative drift speed between the ion species, and their variation matches in situ observations of the fast solar wind found recently by the Wind

spacecraft [*Kasper et al.*, 2013]. Recently, the ubiquitous signatures of kinetic ion instabilities in the solar wind plasma were reconfirmed in Ulysses data [e.g., *Matteini et al.*, 2013]. Although observation of the solar wind exists at 0.29 AU and farther—it is important to measure the properties of the solar wind plasma in the acceleration region close the Sun in order to elucidate the heating and the acceleration mechanism of the solar wind [*McComas et al.*, 2007]. Evidence that Alfvén waves in the chromosphere and the inner corona have sufficient energy to drive the solar wind was obtained from Hinode satellite data [e.g., *De Pontieu et al.*, 2007; *Hahn and Savin*, 2013].

Power law spectra of turbulent magnetic fluctuations in the solar wind near 1 AU were detected in the early days of the space age [e.g., *Coleman*, 1968]. More recent observations of turbulent magnetic fluctuations by Ulysses, Wind, ACE, and Helios spacecraft in the fast solar wind that cover the distances 0.29 AU–5 AU often show the f^{-1} power spectrum of magnetic fluctuations at low (MHD) frequencies in the spacecraft frame, steeper Kolomogorov turbulence $f^{-5/3}$ power spectrum in the ion inertial range and further steeper power laws in the ion dissipation range near the proton gyroresonant frequency, Ω_p [e.g., *Goldstein et al.*, 1995; *Smith et al.*, 2006; *Podesta et al.*, 2006; *Vasquez et al.*, 2007] (see the reviews by *Bruno and Carbone* [2005] and *Alexandrova et al.* [2013]). Recently, Kolomogorov type power spectrum was found in the Alfvénic fluctuations in the inner corona using Doppler velocity data from the Coronal Multichannel Polarimeter (CoMP) instrument [*Tomczyk and McIntosh*, 2009]. Although the energy flux of the Alfvénic fluctuations detected by CoMP is too small to heat the corona—possibly due to instrumental limitations—the observations do suggest that the turbulent Alfvénic fluctuations power spectrum detected in the distant solar wind may have its origin in the inner corona.

The temperature anisotropy of the protons deduced from remote sensing and in situ observations of fast solar wind streams is an indirect evidence for the presence of the ion cyclotron waves in coronal plasma, since the anisotropy can be produced by the resonant absorption of the ion cyclotron waves leading to enhanced perpendicular heating. Purely adiabatic expansion of the solar plasma is expected to result in an opposite effect with decreasing $T_\perp/T_\parallel < 1$. However, $T_\perp/T_\parallel$ is often observed in fast wind streams to be greater than 1 in the heliosphere close to the Sun as was shown in past observations [e.g., *Marsch et al.*, 1982a, 1982b; *Gazis and Lazarus*, 1982; *Hellinger et al.*, 2013]. Theories of ion cyclotron resonance heating have been developed and applied to the solar corona and the solar wind in many past studies [e.g., *Axford and McKenzie*, 1992; *Marsch*, 1992; *Tu and Marsch*, 1997; *Li et al.*, 1999; *Hollweg*, 2000; *Hu et al.*, 2000; *Cranmer*, 2000; *Hollweg and Isenberg*, 2002]. However, the role of parallel-propagating ion cyclotron heating mechanism in coronal heating in multi-ion plasma is not yet fully understood [*Cranmer*, 2000; *Isenberg*, 2004], and oblique waves may play an important role as well [e.g., *Chandran et al.*, 2010; *Isenberg and Vasquez*, 2011].

One-dimensional hybrid simulations of multi-ion solar wind plasma were used to study the heating by parallel-propagating ion cyclotron waves, and the kinetic ion instabilities in the solar wind multi-ion plasma [*Ofman et al.*, 2001; *Liewer et al.*, 2001; *Ofman et al.*, 2002; *Xie et al.*, 2004; *Lu and Wang*, 2005; *Li and Habbal*, 2005; *Hellinger et al.*, 2005; *Ofman et al.*, 2005; *Araneda et al.*, 2009; *Ofman et al.*, 2011; *Maneva et al.*, 2013, 2014]. Solar wind plasma heating by a spectrum of ion cyclotron waves was also studied with 2-D hybrid models that allow more complete description of the interaction between the various wave modes and the inclusion of oblique waves [e.g., *Gary et al.*, 2001, 2003; *Kaghashvili et al.*, 2003; *Hellinger and Trávníček*, 2006; *Gary et al.*, 2006; *Ofman and Viñas*, 2007; *Ofman*, 2010a; *Hellinger and Trávníček*, 2011; *Omidi et al.*, 2014]. Recently, the effect of input Alfvén wave spectrum on solar wind plasma heating was considered in 2-D hybrid models [*Ofman and Viñas*, 2007; *Ofman*, 2010a; *Ofman et al.*, 2011]. The effect of solar wind expansion on the solar wind multi-ion plasma was studied in 1-D hybrid models [*Liewer et al.*, 2001; *Ofman et al.*, 2011; *Maneva et al.*, 2013], and recently in 2-D hybrid model with core and beam protons with He^{++} ions in the distant solar wind near 1 AU [*Hellinger and Trávníček*, 2013].

Here we consider for the first time in 2-D hybrid modeling study the expanding H^+-He^{++} solar wind plasma close to the Sun (with parameters applicable to 10 R_S), the effects of initial He^{++} anisotropy, super-Alfvénic ion relative drift, and a broadband turbulent wave spectrum on the heating of the ions for several values of the expansion parameter. We demonstrate the effects of the solar wind expansion and of the kinetic instabilities produced by the initially nonequilibrium plasma as well as by the driven waves spectrum on the perpendicular ion heating and on the velocity distribution of the ions. The results are relevant to future observations by the Solar Probe+ mission close to the Sun [*McComas et al.*, 2008], and in particular to the proton and He^{++} measurements [*Case et al.*, 2013]. The paper is organized as follows: in section 2 we provide

Table 1. The Initial Parameters of the 2.5-D Hybrid Simulations Cases Described in This Study

Case #	B_{z0}	(ω_1, ω_N) [Ω_p]	Slope p	Expansion Parameter ϵ	$V_d[V_A]$	$T_{\perp,He^{++}}/T_{\parallel,He^{++}}$	$T_{\perp,p}/T_{\parallel,p}$
1a	0			0	0	10	1
1b	0			10^{-4}	0	10	1
1c	0			10^{-3}	0	10	1
2a	0			0	2	1	1
2b	0			10^{-4}	2	1	1
2c	0			10^{-3}	2	1	1
3a	0			0	1.5	1	1
3b	0			10^{-4}	1.5	1	1
3c	0			10^{-3}	1.5	1	1
4a	0.0188	(0.09,0.9)	1	0	0	1	1
4b	0.0188	(0.09,0.9)	1	10^{-4}	0	1	1
4c	0.0188	(0.09,0.9)	1	2×10^{-4}	0	1	1
4d	0.03	(0.09,0.9)	5/3	0	0	1	1
5a	0.0188	(0.09,0.4)	1	0	0	1	1
5b	0.0188	(0.6,0.9)	1	0	0	1	1

the details of the hybrid simulation setup, in section 3 we show the numerical results, and the discussion and conclusions are given in section 4.

2. Simulation Setup

Here we employ the 2.5-D (two spatial directions with three components of velocity and field) hybrid model that treats electrons as massless neutralizing background fluid while the ions are described kinetically using the particle-in-cell approach. The model is an extension of the hybrid code initially developed by *Winske and Omidi* [1993] and *Ofman and Viñas* [2007] and parallelized by *Ofman* [2010a]. The currents, charge density, and the fields are calculated in the 2-D spatial grid of 256×256 computational cell with an average of 127 particles per cell for each ion species, total of 16.6×10^6 particles. We have also performed lower resolution runs and found no significant differences in the results. In the hybrid model each particle is in fact a "super-particle" that corresponds to large number of physical particles with the same phase space location. The numerical ratio between the superparticles and real particles is given by the density normalization. In the present study we use solar wind-like plasma with spatially uniform initial density; i.e., the normalized densities (with respect to the total electron number density) are $n_{He^{++}} = 0.05$, $n_p = 0.9$, and $\left(2n_{He^{++}} + n_p\right)/n_e = 1$ that follows from charge neutrality, where n_e is the electron number density. Cartesian coordinate system is used with the x direction along the uniform background magnetic field $B_0\mathbf{e}_x$. The size of the grid is in units of $\delta x = \delta y = 0.75\Delta$, where $\Delta = c/\omega_{pp}$ is the proton inertia length, and $\omega_{pp} = (4\pi n_p e^2/m_p)^{1/2}$ is the proton plasma frequency. In physical units the inertia length is $\Delta = 2.3 \times 10^7/n_p^{1/2}$ cm. With the solar wind plasma parameters at 10 R_S of $n_p \approx 3 \times 10^3$ cm^{-3} [see, e.g., *Guhathakurta et al.*, 1999] this corresponds to $\Delta \approx 4.2 \times 10^5$ cm, and the simulated area is about $(8 \times 10^7 \text{cm})^2$. The solution is obtained by advancing the particles and fields in time using the Rational Runge-Kutta method [*Wambecq*, 1978] and the Fourier method for spatial solution of the fields on the spatial grid. The boundary conditions are periodic in x and y with the size of the system of 192×192 in units of c/ω_{pp}.

The initial particle distribution in the velocity space is Maxwellian with isotropic temperatures for protons and He^{++} for the driven wave spectrum cases (see Table 1 below). We have considered three forms of initial state that produce ion cyclotron waves: (a) initial bi-Maxwellian distribution for He^{++} ions unstable to the ion cyclotron instability, (b) initially drifting Maxwellian distribution with super-Alfvénic H^+-He^{++} relative drift, and (c) injection of a spectrum of perpendicular magnetic fluctuations at the boundary of the simulated region. Initial states (a) and (b) result in kinetic inabilities that produce a spectrum of ion cyclotron waves in the modeled solar wind plasma, while in initial state (c) the source of the wave spectra is imposed externally at the boundary but propagates self-consistently inside the simulated plasma (see section 2.2 below). The initial temperatures are $\beta_e = 0.021$ and $\beta_{p\parallel} = \beta_{He^{++}\parallel} = 0.041$. The initial state is current free. At present there are no observations of the solar wind plasma parameters at 10 R_S, the anticipated closest approach of the future Solar Probe Plus mission, nor He^{++} parameters in the fast solar wind close to the Sun. However, there are spectroscopic observations in coronal holes from SOHO/UltraViolet Coronagraph Spectrometer that indicate possible large temperature anisotropy of and differential streaming of O^{5+} ions [*Kohl et al.*, 1997;

Raymond et al., 1997; *Cranmer et al.*, 1999] that suggest the extreme valued for He^{++} ions may be plausible in fast wind streams close to the Sun. The large anisotropies and the differential streaming must relax as the solar wind expands to 1 AU to be consistent with in situ observations by ACE [e.g., *Vasquez et al.*, 2007; *Bale et al.*, 2009] and Wind [e.g., *Maruca et al.*, 2011; *Kasper et al.*, 2013].

2.1. Expanding Box Model

In this study we explore the effects of solar wind expansion based on the model proposed by *Grappin and Velli* [1996] for MHD equations and first implemented in 1-D hybrid code by *Liewer et al.* [2001] and in the 2-D hybrid code by *Hellinger et al.* [2003]. Recently, we studied the effects of solar wind expansion in 1-D hybrid model with two ion species [*Ofman et al.*, 2011; *Maneva et al.*, 2013]. Section 2.1 of *Ofman et al.* [2011] and *Maneva et al.* [2013] provide the details on the expanding box equations and their implementation in the 1-D hybrid model. Recently, *Hellinger and Trávníček* [2011] studied the effects of solar wind expansion in the proton beam/core plasma with 2-D hybrid model, and the effects of He^{++} in the expanding distant solar wind was considered by *Hellinger and Trávníček* [2013]. Here we summarize briefly the expanding solar wind equations in the 2-D hybrid model of the H^{+}-He^{++} plasma. The expanding box model assumes radial expansion of the solar wind at a heliocentric distance R_0 of the form $R(t) = R_0 + U_0 t$ with constant velocity U_0. This leads to the definition of an expansion factor

$$a(t) = R(t)/R_0 = 1 + \frac{U_0}{R_0} t = 1 + \epsilon t, \tag{1}$$

where the expansion factor $\epsilon = \frac{U_0}{R_0}$, $\epsilon t \ll 1$, and terms of order ϵ^2 are neglected in the expansion equations. For typical magnetic field strength of 0.01 G at $R_0 = 10\,R_S$ and fast solar wind speed of 750 km s^{-1}, we get $\epsilon \approx 10^{-5}$ where the time is in units of the proton gyrofrequency Ω_p^{-1}. However, due to numerical limitations on the computation time in the hybrid model we use at least an order magnitude larger values of ϵ, consistent with past studies. The coordinates in the expanding frame become time dependent:

$$x' = x + R(t),\ y' = a(t)y,\ z' = a(t)z. \tag{2}$$

The above transformations are used to derive the velocities in the moving and expanding frame that relate to the rest frame:

$$v_x' = v_x - U_0,\ v_y' = v_y - \epsilon y'\ v_z' = v_z - \epsilon z', \tag{3}$$

and the electromagnetic fields in the expanding frame are given in *Ofman et al.* [2011] and *Maneva et al.* [2013] and implemented in our hybrid codes. In the 2.5-D hybrid code, all three components of velocities and fields are maintained as well as their spatial dependence on x' and y', but the derivatives with respect to z' are taken to be zero. For simplicity, in the following sections we drop the primes.

2.2. Driven Wave Spectrum

The heating of solar wind plasma by a temporally driven waves spectrum with 2-D hybrid code was studied recently [*Ofman and Viñas*, 2007; *Ofman*, 2010a; *Ofman et al.*, 2011]. At present it is not computationally feasible to model MHD turbulent cascade that occurs on large scales compared to kinetic scales modeled in a hybrid code. Therefore, a turbulent wave spectrum is introduced as an external source in the hybrid model. The present approach is based on the approach used by *Ofman* [2010a] and *Ofman et al.* [2011] of driven circularly polarized Alfvén waves spectrum. In these previous studies the Alfvén waves were driven as temporal fluctuation with a prescribed spectral slope with frequencies below the proton gyroresonant frequency Ω_p uniformly at the boundary of the simulation region. Part of the left-hand polarized parallel-propagating wave spectrum resonates with the ions when the resonant condition $\omega - k_{\|} V_{i\|} = \Omega_i$ is met in the plasma [*Stix*, 1962]. This time-dependent approach is alternative to other methods that initiate the hybrid model particle velocities and fields with a spectrum of Alfvénic fluctuations at $t = 0$ and let it evolve self-consistently with time [e.g., *Liewer et al.*, 2001; *Maneva et al.*, 2013]. The main difference between the two methods is that the free energy is supplied continuously and gradually to the plasma in the present time-dependent driver method, while in the initial value approach the spectrum of fluctuations with its total power is embedded in the plasma at $t = 0$.

Here we extend the time-dependent driver method by imposing nonuniform magnetic fluctuations at the boundary with a spatially (y) dependent random phase, given by

$$B_z(t, x = 0, y) = B_{z0} \sum_{i=1}^{N} a_i \sin(\omega_i t + \Gamma_i(y)), \tag{4}$$

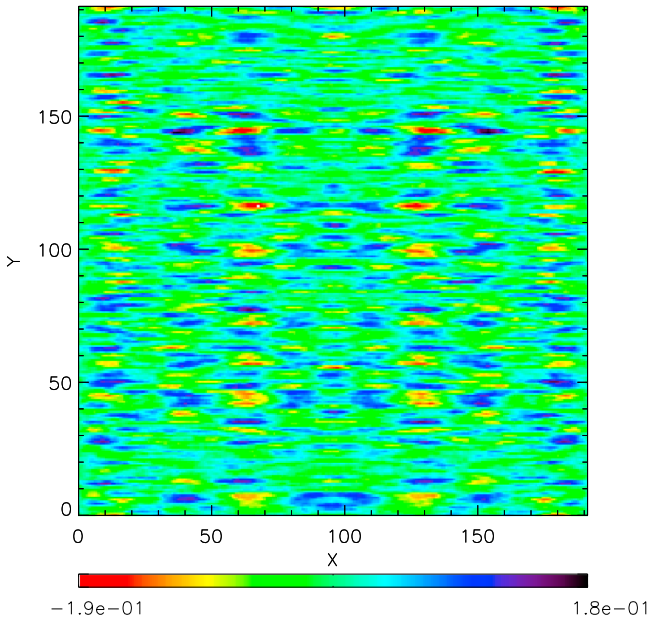

Figure 1. The magnetic fluctuations (B_z) in the x-y plane at the final quasi-steady stage of the driven wave spectrum (Case 7). The symmetry due to the periodic boundary conditions is evident. An animation of this figure is available in the electronic version of this journal.

where the i'th mode amplitude is $a_i = i^{-p/2}$, p is the parameter that determines the slope of the power spectrum (the values $p = 1$ and $p = 5/3$ were used), the frequency $\omega_i = \omega_1 + (i-1)\Delta\omega$, the frequency range $\Delta\omega = (\omega_N - \omega_1)/(N-1)$, $\Gamma_i(y)$ is the y-dependent random phase, N is the number of modes, and B_{z0} is the amplitude. The number of modes was $N = 300$. In a hybrid code the magnetic field is in arbitrary units that can be related to physical units by a choice of the field strength and density units. The value of the random phase is in the range $(0, 2\pi)$, and it is varied at each y grid location. This ensures that the Alfvén waves launched at the boundary have a nonuniform (uncorrelated) wavefront. The value of the B_{z0} parameter was varied and is given in Table 1 below. The periodic boundary condition in the x direction results in the periodic application of the driver at the x boundaries, since the application of the magnetic fluctuations at the first grid point ($x = 0$) are essentially reproduced at the penultimate grid point ($x = x_{max} - \delta x$, where $x_{max} = 256\delta x$) due to the application of the boundary conditions. While the value of B_z is imposed by the driver in equation (4), the values of B_x and B_y at the boundaries are calculated self-consistently by using the Maxwell and Lorentz equations, i.e., the particle motions and positions are used to calculate the net currents, that contain the effects of the imposed B_z from the previous time step.

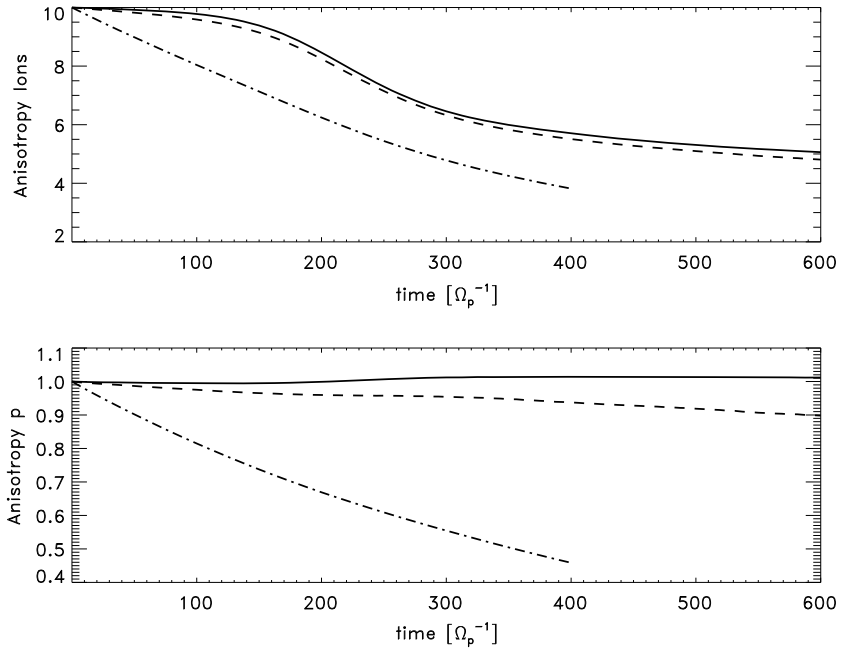

Figure 2. The temporal evolution of the temperature anisotropy of He^{++} (top) ions and (bottom) protons for non-expanding solar wind (solid) and for expanding solar wind with the expansion parameters $\epsilon = 10^{-3}$ (dash-dotted), and $\epsilon = 10^{-4}$ (dashes).

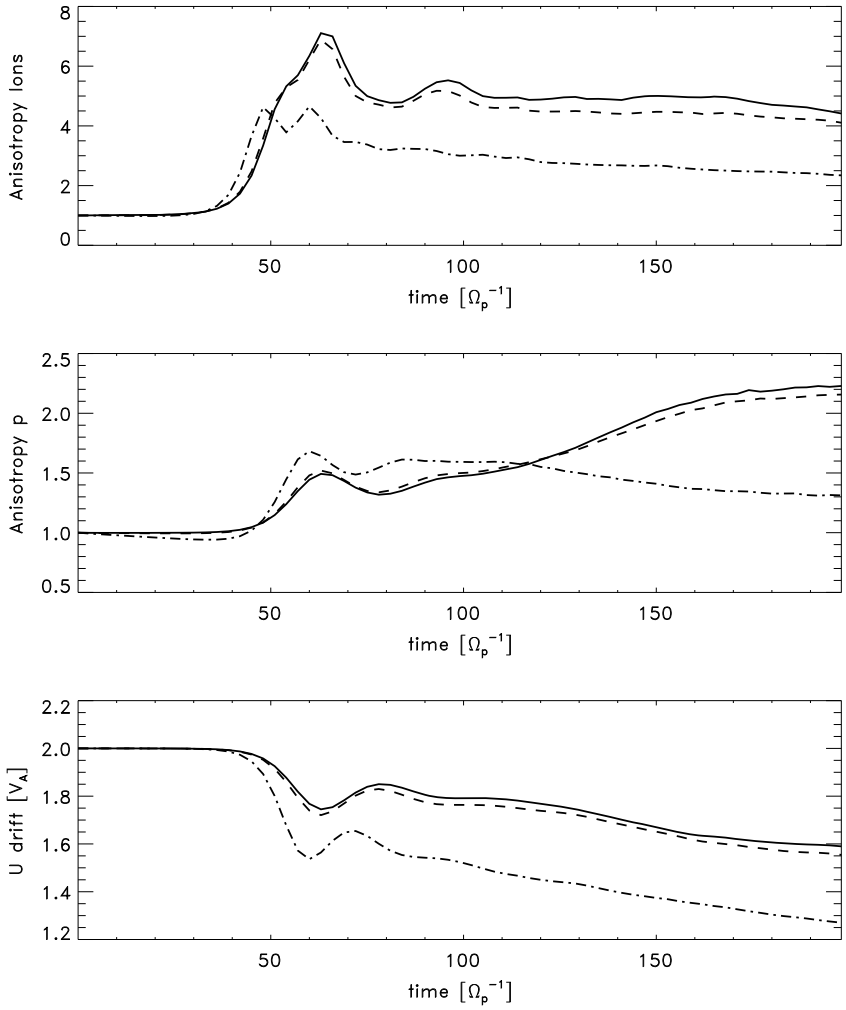

Figure 3. The temporal evolution of the temperature anisotropy of He^{++} (top) ions, (middle) protons, and (bottom) the drift velocity for nonexpanding solar wind (solid) and for expanding solar wind with the expansion parameters $\epsilon = 10^{-3}$ (dash-dotted), and $\epsilon = 10^{-4}$ (dashes). The initial drift was $2\,V_A$ in initially isotropic plasma.

The interior of the computational domain is calculated fully self-consistently by solving the hybrid model equations. A snapshot of the B_z fluctuations in the quasi-steady state of the evolution is shown in Figure 1, with the animation available as supporting information.

3. Numerical Results

The results of the 2.5-D hybrid modeling are shown in Figures 1–12, and the initial parameters of the various cases in this study are listed in Table 1. In order to excite a spectrum of ion cyclotron waves we initiate the He^{++} population with $T_{i,\perp}/T_{i,\parallel} = 10$ (Case 1) that is unstable with respect to the ion cyclotron mode for the chosen values of $\beta_{He^{++}\parallel} = 0.041$ and $n_{He^{++}}/n_e$ [e.g., *Gary et al.*, 2001]. Figure 2 shows the temporal evolution of the temperature anisotropy for protons and He^{++} ions with an initial anisotropic bi-Maxwellian He^{++} populations and initially isotropic protons. The solid curves show the evolution without expansion ($\epsilon = 0$), the dashed curve is for the expanding solar wind with $\epsilon = 10^{-4}$, and the dot-dashed curve is for the case with $\epsilon = 10^{-3}$. Note that in case of $\epsilon = 10^{-3}$ the results are shown to $t = 300\Omega_p^{-1}$, since beyond this time the approximation $\epsilon t \ll 1$ becomes less appropriate. However, for $\epsilon = 10^{-4}$ the approximation is valid throughout the evolution time. It is evident that the He^{++} temperature anisotropy decreases rapidly in agreement with previous 2-D hybrid modeling results [e.g., *Gary et al.*, 2001], while the proton anisotropy remains near unity in the nonexpanding plasma. The effect of expansion is evident in the further decrease

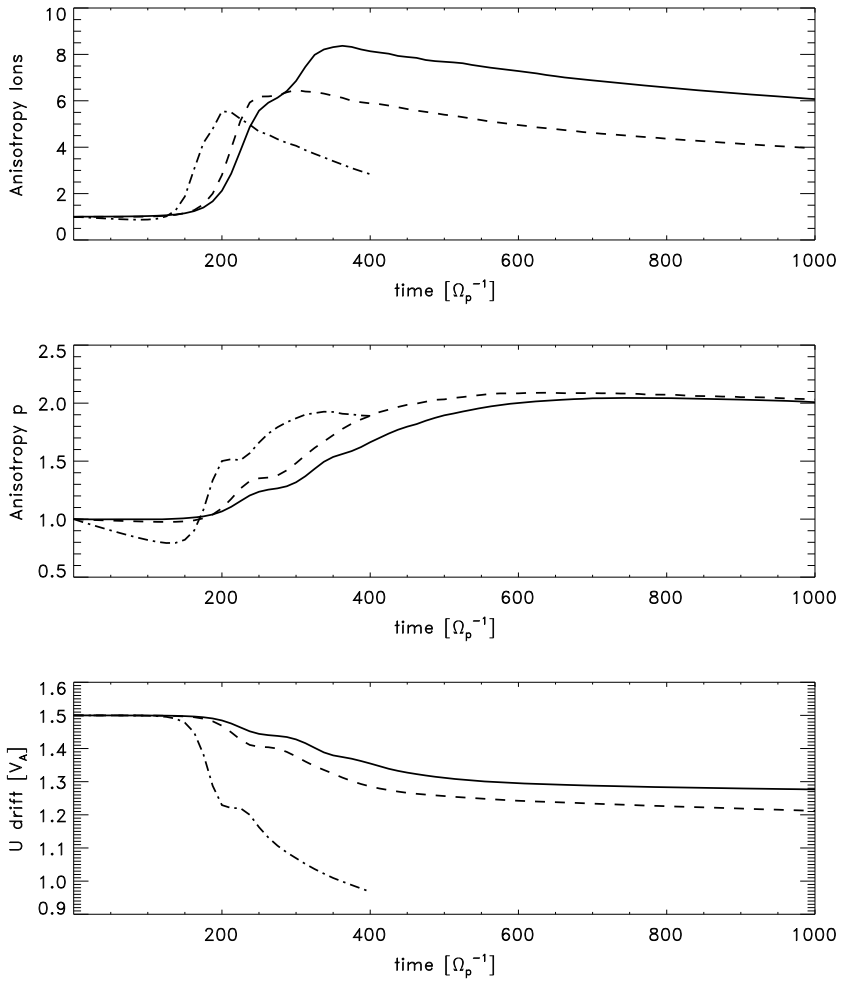

Figure 4. Same as Figure 3 but with an initial drift 1.5 V_A and longer run.

of the anisotropy with time compared to the nonexpanding case due to the perpendicular cooling, and this effect is amplified for the rapid expansion case ($\epsilon = 10^{-3}$).

The temporal evolution of the temperature anisotropy of He^{++}, protons, and the relative drift velocity are shown in Figure 3. The nonexpanding case is shown for reference with the solid curve, and the evolution is in agreement with previous 2-D hybrid modeling studies [e.g., *Ofman and Viñas*, 2007]. The initial drift is super-Alfvénic with $V_d = 2\,V_A$ (Case 2) unstable to the magnetosonic drift instability [*Gary*, 1993] and results in the relaxation of the drift and the emission of the ion cyclotron waves. These waves lead to the resonant perpendicular heating of the protons and He^{++} ions as evident in the evolution of the anisotropies. The proton temperature anisotropy increases to 2.2 at the end of the run, while the He^{++} is rapidly heated perpendicularly to an anisotropy > 7. However, the high He^{++} anisotropy results in secondary instability and the ultimate decrease of the anisotropy to lower values at $t = 200\Omega_p^{-1}$. Consistent with the expected evolution, the expansion of the solar wind plasma results in faster decrease of the drift and the final anisotropy reaches lower values.

In Figure 4 we show the evolution of the temperature anisotropy for protons and He^{++} ions for the initially drifting H^+-He^{++} population at $V_d = 1.5\,V_A$ (Case 3). The longer duration of the run ($t = 1000\Omega_p^{-1}$) compared to the case shown in Figure 3 is necessary due to the slower evolution of the instability due to the lower drift velocity case, closer to marginal stability at $V_d = V_A$. It is evident toward the end of the run that for nonexpanding plasma the drift is relaxing and the anisotropy of protons and He^{++} ions is decreasing from a peak value of ~8.4 to higher values than in the expanding case. This is accompanied by the increase of the proton temperature anisotropy, peaking at values ~2 for the nonexpanding and the expanding cases and decreasing slightly toward the end of the run. When expansion is considered the peak anisotropy occurs at

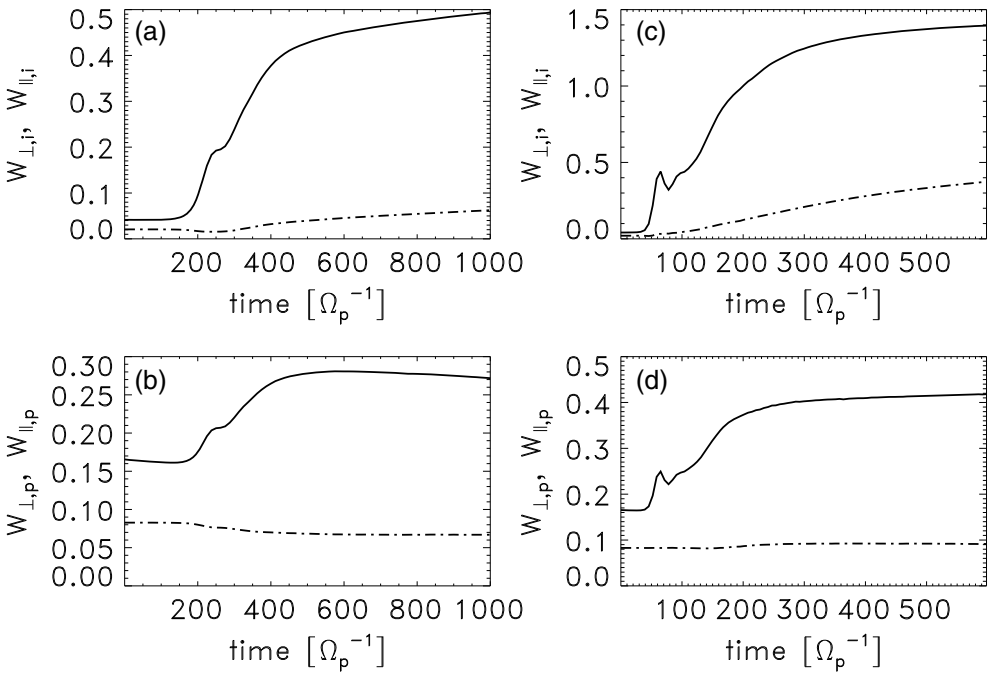

Figure 5. The temporal evolution of the perpendicular (solid) and parallel (dashes) energies for expanding solar wind plasma with the expansion parameter $\epsilon = 10^{-4}$. (a) He^{++} with the initial drift 1.5 V_A. (b) H^+ with the initial drift 1.5 V_A. (c) He^{++} with the initial drift 2 V_A. (d) H^+ with the initial drift 2 V_A.

earlier times than in the nonexpanding case. This process is most rapid (among the cases considered) when $\epsilon = 10^{-3}$, shown within the time frame of validity, since the inflation of the perpendicular coordinates with time in the expanding box model results in the decrease of the perpendicular velocities of the ions, equivalent to perpendicular cooling (see section 2.1). Thus, these cases demonstrate that expansion plays an important role in accelerating the evolution of the magnetosonic drift instability, as well as the subsequent resonant heating of the protons and He^{++} ions compared to the nonexpanding drifting case. Expansion also causes small reduction in the cyclotron frequencies by a factor of $a(t)^{-2}$ due to the gradual decrease of the background magnetic field [see *Liewer et al.*, 2001], decreasing the difference in resonant frequencies between protons and He^{++} ions by the same factor, and may become important in marginally stable case shown in Figure 4, increasing the coupling between the protons and ions, and resulting in more rapid heating of protons compared to the nonexpanding case.

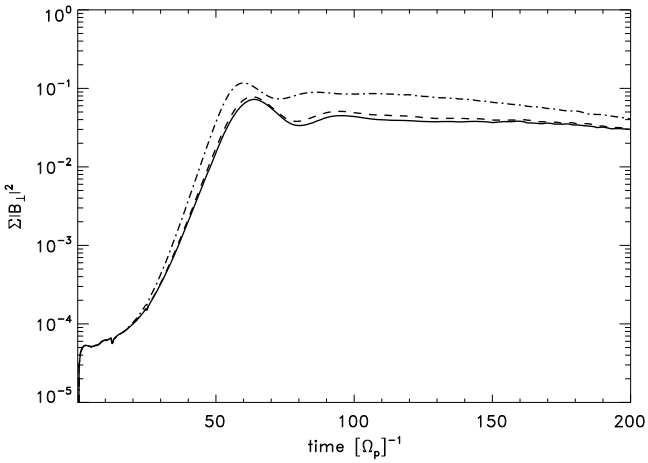

Figure 6. The temporal evolution of the perpendicular magnetic fluctuations $|\delta B_\perp|^2$ for the solar wind H^+ -He^{++} plasma with initial drift $V_d = 2\,V_A$ with $\epsilon = 0$ (solid), $\epsilon = 10^{-4}$ (dashes), $\epsilon = 10^{-3}$ (dash-dotted).

In Figure 5 the temporal evolution of the parallel ($W_\parallel$) and the perpendicular ($W_\perp$) energies is shown for the H^+-He^{++} drifting cases with initial drift $V_d = 1.5\,V_A$ (Case 3) and $V_d = 2\,V_A$ (Case 2). The expansion factor was $\epsilon = 10^{-4}$. This value is shown since it is closer to the real expansion rate at 10 R_S than $\epsilon = 10^{-3}$. It is evident that the ions are heated in the perpendicular direction as the drift velocity is decreasing. The parallel energies remain small compared to the perpendicular energies and do not vary significantly for protons, while showing small increase for He^{++}. This is consistent with the expected evolution due to the

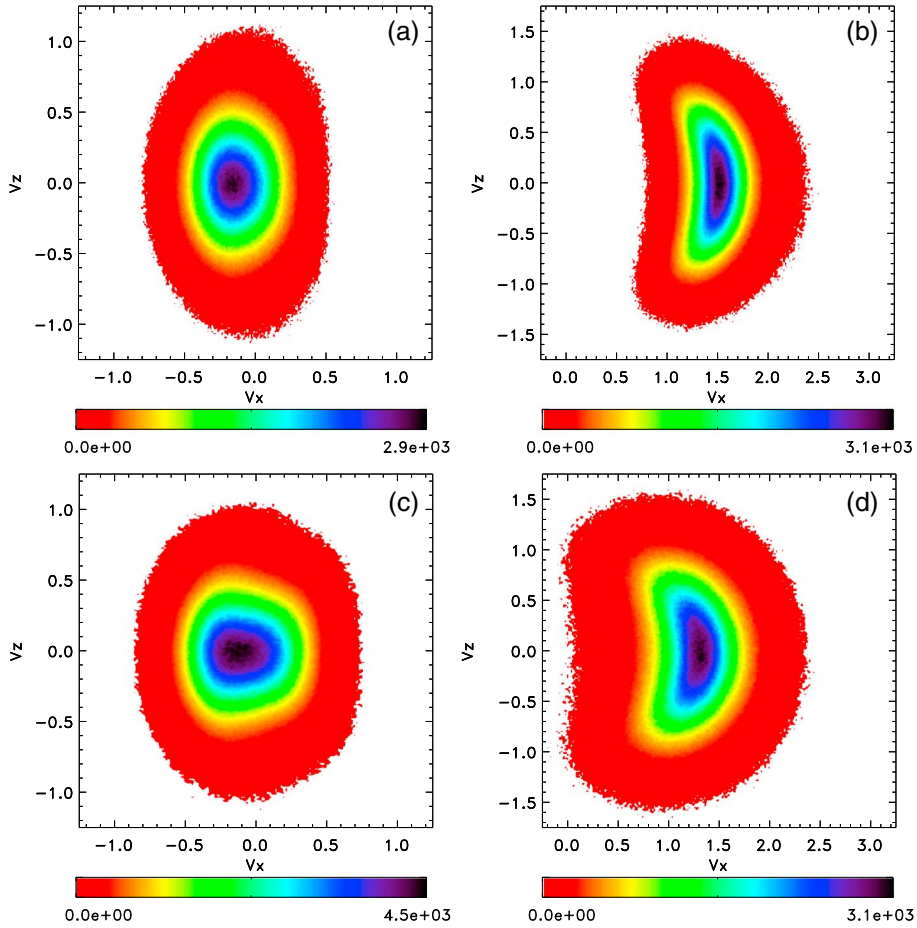

Figure 7. A snapshot of the $V_x - V_z$ phase space plot with an initial drift of $2\,V_A$ (Case 2) at $t = 200\Omega_p^{-1}$. (a) H^+ without expansion. (b) He^{++} without expansion. (c) H^+ for expanding solar wind plasma with $\epsilon = 10^{-3}$. (d) He^{++} for expanding solar wind plasma with $\epsilon = 10^{-3}$.

magnetosonic drift instability that results in the emission of the ion cyclotron spectrum of waves that resonate with the ions and increase in the magnetic fluctuations energy summed over the simulation region $\Sigma_{x,y}|\delta B_\perp|^2$ (see Figure 6). The results are consistent with previous studies of the magnetosonic drift instability [e.g., *Araneda et al.*, 2002; *Xie et al.*, 2004; *Ofman and Viñas*, 2007]. We find that the effect of solar wind expansion is small in this case and does not change the qualitative evolution of the parallel and perpendicular energies.

The $V_x - V_z$ plane of the velocity phase space for protons and He^{++} ions is shown in Figure 7 for the expanding and nonexpanding cases with drift $V_d = 2\,V_A$ (Case 2) at $t = 200\Omega_p$. It is evident that the expansion resulted in faster relaxation of the drift (V_x) and larger perpendicular heating in the He^{++} ions compared to the nonexpanding case. The "donut-shaped" velocity distribution is clearly non-Maxwellian, with the hotter ions having smaller drift compared to the colder species. For protons, the perpendicular heating is evident as well with smaller effect for the expanding case. However, the non-Maxwellian departures are less pronounced in the proton velocity distributions in the expanding and nonexpanding cases.

Figure 8 is devoted to the perpendicular velocity distribution $V_y - V_z$ for protons and He^{++} for the drifting case with $V_d = 2\,V_A$ (Case 2) at $t = 200\Omega_p^{-1}$ with and without expansion. The He^{++} perpendicular velocity distribution in Figure 8a is nearly circular and is close to Maxwellian for the core of the distribution with faster than Maxwellian decrease at the tails, as evident in the best fit plot (Figure 8b). When expansion is present, the core of the distribution becomes depleted relative to Maxwellian (Figures 8c and 8d), while without expansion this effect is evident at later times in the nonexpanding case (not shown). The proton perpendicular velocity distribution is very close to Maxwellian as evident in the phase space Figure 8e and in the best fit Maxwellian plot Figure 8f.

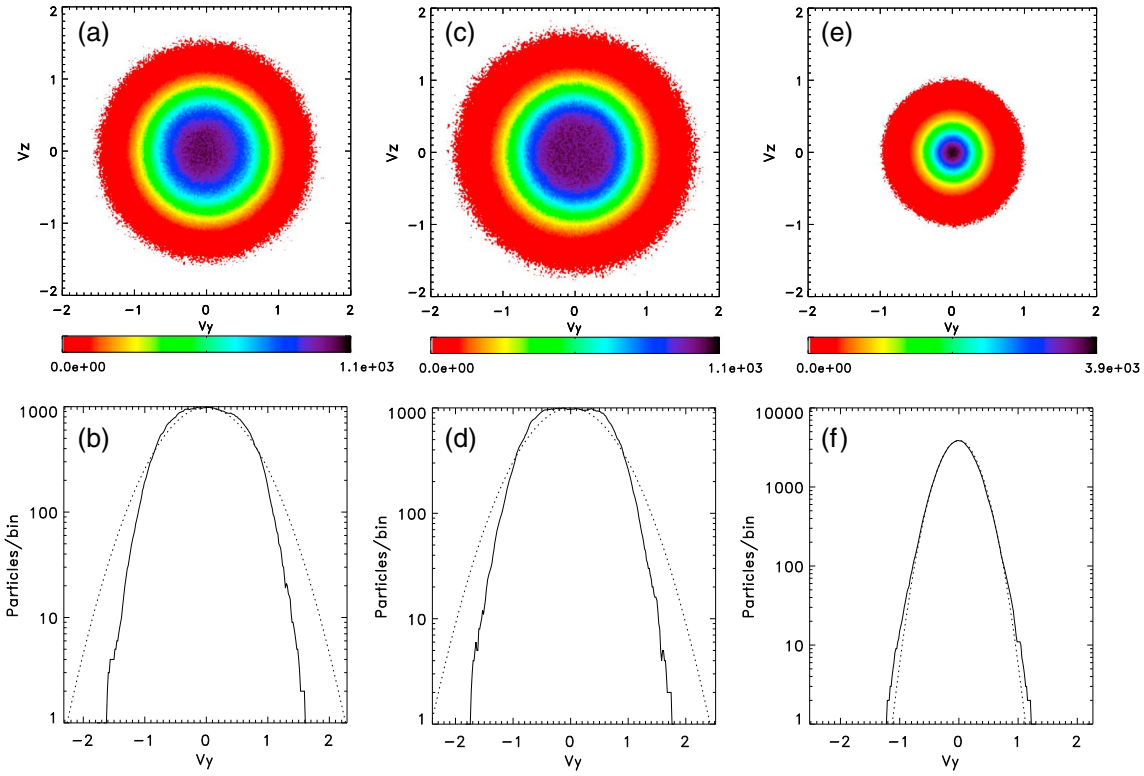

Figure 8. Perpendicular velocity distributions with an initial drift of 2 V_A at $t = 200\Omega_p^{-1}$ for He^{++}. (a) A snapshot of the $V_y - V_z$ phase space without expansion. (b) The particle velocity distribution at $V_x = 0$. The best fit Maxwellian velocity distribution is shown with the dotted line. (c) Same as Figure 8a but with expansion $\epsilon = 10^{-3}$. (d) Same as Figure 8b but with expansion $\epsilon = 10^{-3}$. (e) Same as Figure 8c for protons. (f) Same as Figure 8d for protons.

The perpendicular magnetic fluctuation power spectrum for the nonexpanding and the expanding solar wind plasma with an initial drift $V_d = 2\,V_A$ (Case 2) is shown in Figure 9. The values shown were obtained by averaging the power spectra of magnetic fluctuations in 10 × 10 cells in the center of the simulated region to reduce statistical noise. It is evident that for frequencies $> 0.5\Omega_p$ the spectral intensity has nearly power law dependence. The peak of the emission occurs at about $0.5\Omega_p$, consistent with the He^{++} gyroresonant emission due to the drift instability. In the nonexpanding plasma the best fit slope of the power law spectrum is −2.1. When expansion is introduced the slope of the power law spectrum is nearly the same (−2.0) and the peak power is shifted to slightly lower frequency indicating small effect of the expansion on the power law dependence.

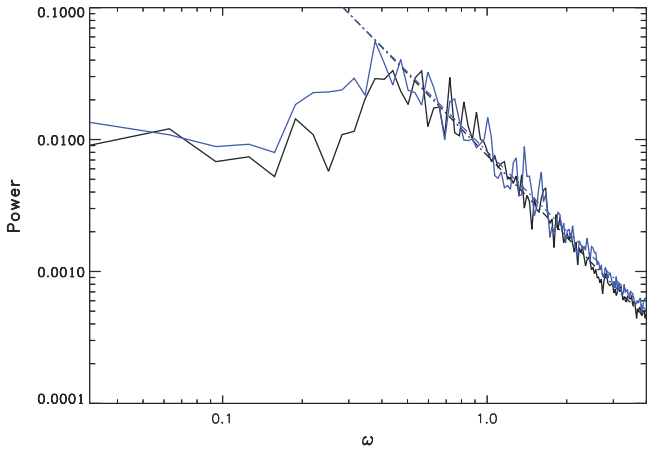

Figure 9. The power law spectrum of magnetic fluctuations for the H^+ -He^{++} solar wind plasma with an initial drift 2 V_A. Nonexpanding case (black) with best fit power law. Expanding case (blue) with $\epsilon = 10^{-3}$ and the best fit power law. The power law fits are −2.1 for the nonexpanding case and −2.0 for the expanding case. The plot shows the average of power spectra in 10 × 10 cells area in the center of the simulated region to reduce statistical noise.

Figure 10 is devoted to the results of the modeling of the solar wind plasma with a driven wave spectrum given by equation (4) and imposed at the boundary (Case 4). In Cases 4a–4c we show the results for f^{-1} input power spectrum, with and without expansions, and in Case 4d the results are for $f^{-5/3}$ input power spectrum without expansions. The effects of solar wind expansion are considered by comparing the expanding solutions to the

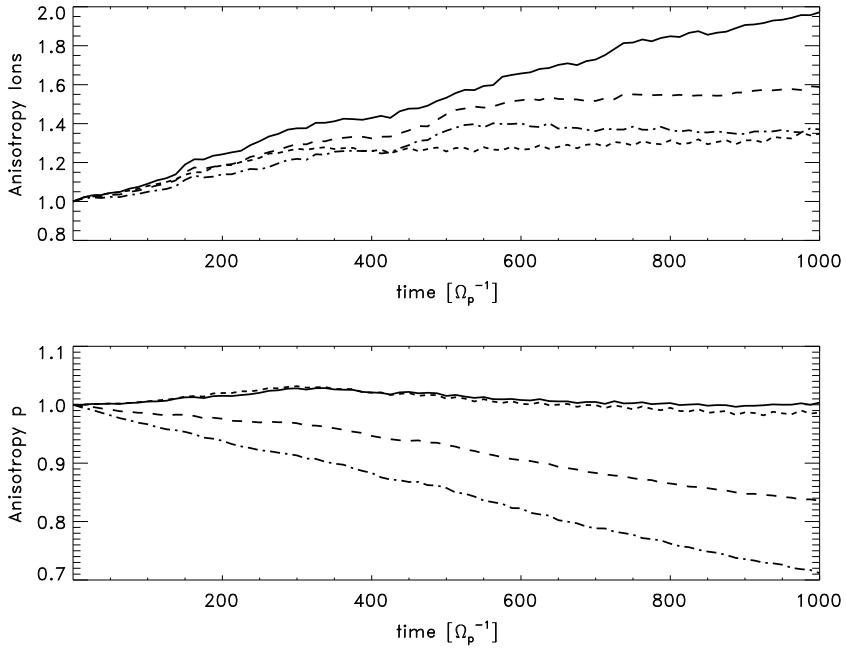

Figure 10. The temporal evolution of the temperature anisotropy of He^{++} (top) ions and (bottom) protons for solar wind plasma heated by input broadband spectrum of Alfvén waves of the form f^{-1} in nonexpanding solar wind (solid) and in expanding solar wind with $\epsilon = 10^{-4}$ (dashes) and with $\epsilon = 2 \times 10^{-4}$ (dash-dotted). The evolution of He^{++} anisotropy for Kolmogorov $f^{-5/3}$ driving spectrum is shown (short dashes).

nonexpanding case. When $\epsilon = 0$ it is evident that the injected spectrum results in strong perpendicular heating of the He^{++} ions as their temperature anisotropy is above 2 at the end of the run, with small perpendicular heating of the protons. The H^+-He^{++} drift produced by the heating is negligible compared to V_A (not shown). When expansion is introduced the final perpendicular heating and the resulting anisotropy of He^{++} is reduced to 1.6 for $\epsilon = 10^{-4}$ and to 1.35 for $\epsilon = 2 \times 10^{-4}$, consistent with the expected evolution. The proton anisotropy is strongly affected by the perpendicular cooling due to the expansion since the input wave spectrum does not contribute to their perpendicular heating that offsets the effect of expansion in the case of He^{++} ions. Therefore, the final proton temperature anisotropy reduces to 0.99 for $\epsilon = 10^{-4}$ and to 0.7 for $\epsilon = 2 \times 10^{-4}$ at the end of the run. For the low-$\beta_{p\|} = 0.041$ case considered here these values of the temperature anisotropies do not lead to instability. In Case 4d the He^{++} heating is reduced due to lower power in the resonant range (compared to Case 4a) in the steeper power spectrum. Observations show that for this value of $\beta_{p\|}$ the proton anisotropy can be as low as $T_{p\perp}/T_{\|} = 0.15 - 0.2$ at 1 AU, and these values correspond to low magnitude of magnetic fluctuations $|\delta B/B_0| << 1$ [*Bale et al.*, 2009; *Maruca et al.*, 2011]. The high values of proton anisotropy in these observations correlate with increased $|\delta B/B_0|$ and can be interpreted as evidence of enhanced perpendicular proton heating by the resonant waves.

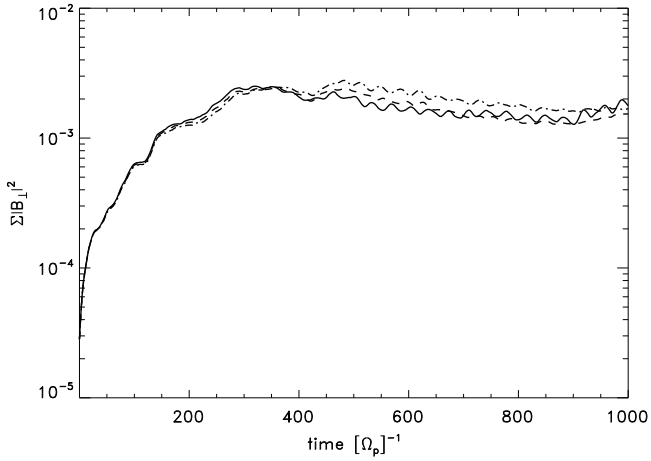

Figure 11. The temporal evolution of the total perpendicular magnetic fluctuations for the cases with f^{-1} input wave spectrum shown in Figure 10. Nonexpanding solar wind (solid), expanding solar wind with $\epsilon = 10^{-4}$ (dashes), and with $\epsilon = 2 \times 10^{-4}$ (dash-dotted). A smoothing was applied to the curves to remove high-frequency noise.

We note that the proton heating is small in Cases 4a–4c due the combination of

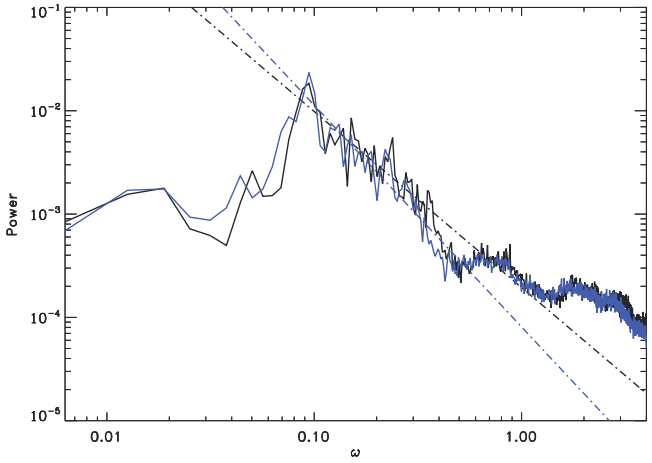

Figure 12. The power spectrum of the magnetic fluctuations for the driven Cases 4a and 4b. Nonexpanding solar wind (black) and expanding solar wind with $\epsilon = 10^{-4}$ (blue) power spectra of perpendicular magnetic fluctuations are shown. The power law fits are −1.68 for the nonexpanding case and −2.14 for the expanding case. The plot shows the average of power spectra in 10×10 cells area in the center of the simulated region to reduce statistical noise.

a broad frequency range for the driven magnetic fluctuations with the steepness of the driven spectral slope. Indeed, if we narrow down the frequency band of the driver, keeping the same total amplitude for the magnetic field fluctuations that would leave more power for wave-particle interactions in this frequency range. If we restrict the driven spectra to lower frequencies, in the range $\omega_1 = 0.09$, $\omega_N = 0.4$ (Case 5a; note that for computational reasons the test Case 5 was run at lower spatial resolution of 128×128), that means we start with more overall wave energy close to the He^{++} resonance scales and hence we end up with higher heating and anisotropy for the He^{++} and practically no proton heating. When we introduce higher-frequency band of the driver ($\omega_1 = 0.6$ and $\omega_N = 0.9$, Case 5b), this increases the probability for wave-particle interaction with the protons and in this case we observe simultaneous significant proton and He^{++} ions perpendicular heating. We should note that on a long term (~1000 gyroperiods) the expansion with $\epsilon = 10^{-4}$ in the case of lower frequency spectrum can lead to an increase in the perpendicular heating and the temperature anisotropy for the He^{++} ions. This can be best understood by the concept that although, in general, the adiabatic expansion leads to perpendicular cooling for both species, it can also support a transition from initially low-frequency nonresonant modes into resonant ones with the He^{++} ions, thus facilitating direct cascade and helping energy transfer toward small scales. The results above describe the case with initial spectral slope −1, while further increase of the steepness of the input wave spectrum slope decreases further the available energy for the proton heating.

The total perpendicular magnetic fluctuations, $\Sigma|B_\perp|^2$, for the three Cases 4a–4c are shown in Figure 11, indicating that after initial transient the magnitude of the fluctuations reaches nearly steady level at similar values. The saturation of the magnetic fluctuations level is the result of the absorption of the driven

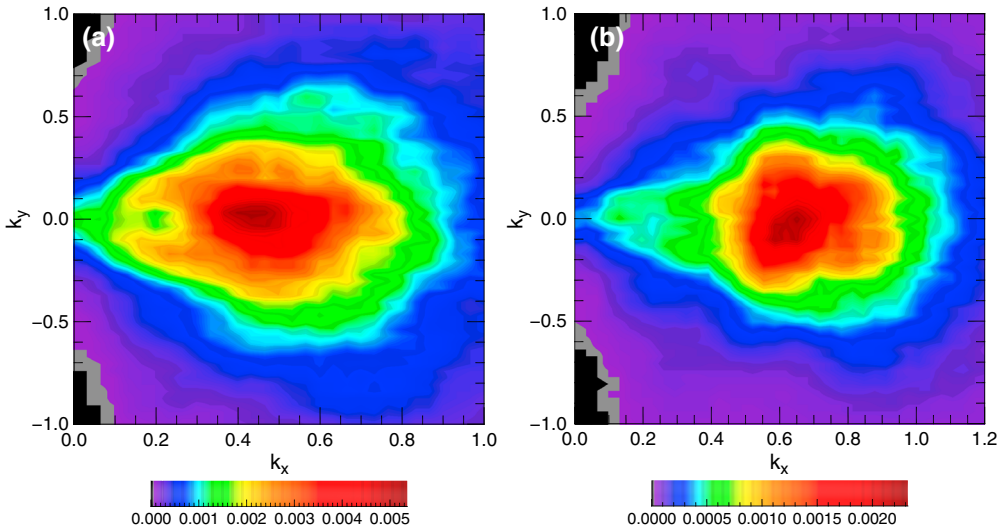

Figure 13. The two-dimensional power spectrum (k_x-k_y plane) of the spatial magnetic fluctuations for (a) Case 2b and (b) Case 3b at the end of the run. The presence of the oblique waves is evident as the power in the region $|k_y| > 0$ is significant for both cases.

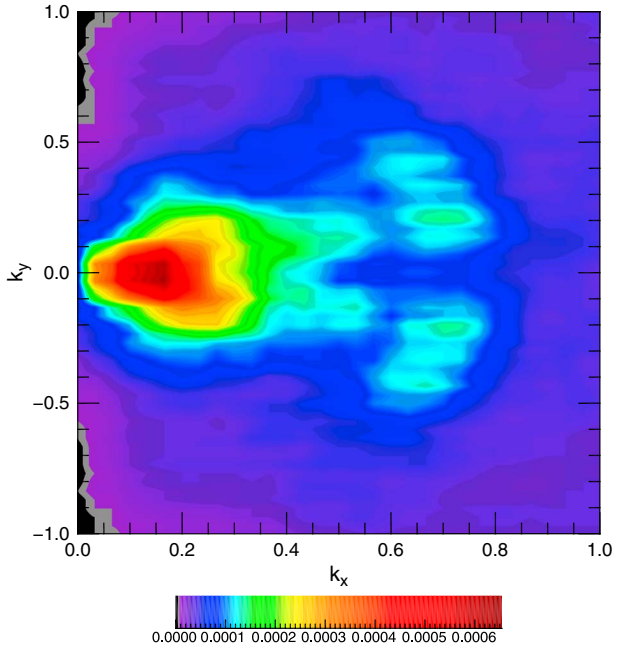

Figure 14. The two-dimensional power spectrum (k_x-k_y plane) of the spatial magnetic fluctuations for the Case 4b at the end of the run. The presence of the oblique waves is evident as the power in the region $|k_y| > 0$.

magnetic fluctuations by the particle population, leading to nearly balance steady state. The increased values of the expanding cases compared to the case without expansion is due to the decreased absorption by the ions as evident in decreased perpendicular heating in the expanding solar wind plasma compared to the nonexpanding case, leading to higher net level of unabsorbed magnetic fluctuations.

The power spectrum of the magnetic fluctuations in the center of the simulated region is shown in Figure 12 for nonexpanding (black) and expanding (blue) solar wind plasma with driven spectrum of fluctuations at the boundary (Cases 4a and 4ab). The dip in the spectrum around $\omega = 0.5\Omega_p = \Omega_{He^{++}}$ is consistent with the resonant absorption by the thermal population of He^{++}. Smaller absorption dip in the spectrum is evident near $\omega = \Omega_p$, with further small variation possibly due to hybrid resonances. It is evident that the spectrum steepens significantly in the expanding case ($\epsilon = 10^{-4}$) and the slope steepens from −1.61 to −2.11 in the sub-ion gyroresonance region (0.09–0.4), both steepen with respect to the slope of −1 for the input magnetic fluctuations at the boundary. As the waves are injected on the side of the computational box the magnetic fluctuations travel toward the inner part of the computational region, where the spectra evolve, some power is being transmitted to the particles and new waves are generated. Thus, the power spectrum varies with position, with a spectral slope very close to −1 at the x boundaries, which further steepens to over −2 toward the center of the computational region, as a result of turbulent cascade, wave absorption, wave-particle interactions, and expansion. These results are consistent with the perpendicular heating and magnetic energy differences between the expanding and nonexpanding cases.

The two-dimensional spectra of magnetic fluctuations for the streaming Cases 2b and 3b with expansion ($\epsilon = 10^{-4}$) are shown in Figure 13 at the end of the runs. It is evident that the peak power is concentrated in the parallel direction near the $k_y = 0$ axis. However, significant power is also present in the plane in the region $|k_y| > 0$. The streaming instability produces not only mostly parallel but also oblique waves in agreement with the solution of the linear Vlasov dispersion relation for warm plasma and super-Alfvenic proton-He^{++} differential streaming [see *Ofman and Viñas*, 2007, Figure 2]. Additional power in oblique waves is generated due to wave-particle interactions and scattering in the nonlinear stage of the evolution of the instability. This is also supported by the two-dimensional spectrum of the spatial magnetic fluctuations due to the injected waves (Case 4b) shown in Figure 14. It is evident that the wave power peaks near the $k_y = 0$ axis in this case as well. However, here as well significant power is evident in the region $|k_y| > 0$ indicating nonlinear scattering of the waves to oblique directions. The spectra of the spatial magnetic fluctuations also show that most of the power is localized at $|k| < 1$ due to the strong damping of the waves at higher k's in warm plasma, consistent with Vlasov dispersion in warm proton-He^{++} plasma [e.g., *Davidson and Ogden*, 1975; *Gary*, 1993; *Ofman and Viñas*, 2007].

4. Discussion and Conclusions

Using 2-D hybrid expanding box model of the solar wind plasma, we investigate the ion heating of multicomponent solar wind by the ion cyclotron and drift instabilities, as well as by a turbulent power law spectrum of Alfvén waves injected at the boundary of the simulated region. The heating processes can account for the enhanced (compared to proton) He^{++} ion heating and preferential acceleration observed in situ by Helios, Ulysses, ACE, and Wind spacecraft. The drift may result from ion beams that are formed due to

differential acceleration and preferential heating to a more than mass-proportional temperature ratio from parametric instability of large-amplitude Alfvén waves [e.g., *Araneda et al.*, 2009; *Maneva et al.*, 2013], while the ion heating may result from the magnetosonic drift instability and the absorption of the resonant part of a turbulent power law wave spectrum with little effect from solar wind radial expansion, demonstrated in this study. While the perpendicular temperature anisotropy for the He^{++} ions is increasing due to the absorption of resonant waves, the velocity phase-space diffusion and pitch angle scattering lead to eventual transfer of the energy to the parallel direction and increase in parallel temperature of the ions, reducing the final temperature anisotropy.

When the initial drift is super-Alfvénic , $V_d > V_A$, the He^{++} ion perpendicular velocity distribution becomes non-Maxwellian, and He^{++} temperature develop strong perpendicular anisotropy. This anisotropy further relaxes through the ion cyclotron instability, emitting waves that subsequently lead to perpendicular proton heating. We find that the relaxation of an initially super-Alfvénic ion relative drift produces magnetic fluctuations spectrum with power law form close to f^{-2} where the steepening of the spectrum is typical of the dissipation range. The power law spectrum becomes somewhat steeper when rapid solar wind expansion is considered. We find that the solar wind expansion leads to faster evolution of the magnetosonic drift instability compared to the nonexpanding case, and faster generation of the perpendicular magnetic fluctuations, that resonantly heat the ions. The development of oblique waves is evident in the magnetic fluctuations 2-D power spectrum.

We compare the perpendicular heating due to the injected f^{-1} spectrum in expanding and nonexpanding solar wind plasma, and we find that the expansion reduces the final perpendicular anisotropy of He^{++} ion population. We compare the perpendicular heating due to $f^{-5/3}$ injected spectrum with the f^{-1} spectrum (with similar total energies) and find that the perpendicular heating of the He^{++} ions is reduced. This is due to the fact that the steeper $f^{-5/3}$ contains less energy in the high-frequency band that resonates with the He^{++} ions. The presence of significant power in oblique waves is demonstrated in 2-D power spectrum for the driven spectrum case.

The effect of solar wind expansion is considered with the expanding box model in the 2-D hybrid code. In general, we find that the solar wind expansion does not strongly affect the heating of the solar wind He^{++} ions in the acceleration region of the solar wind on the modeled time scales. The solar wind radial expansion can reduce dramatically the anisotropy of protons leading to $T_{p\perp}/T_{p\parallel} < 1$ in the expanding acceleration region of the solar wind. For low-$\beta_{p\parallel}$ values this is consistent with in situ observations that find low proton anisotropy associated with low magnetic fluctuations [*Bale et al.*, 2009; *Maruca et al.*, 2011]. Thus, our results agree with the observationally based conclusions that the higher values of $T_{p\perp}/T_{p\parallel} \geq 1$ in the solar wind require enhanced perpendicular heating that can be provided by resonance with turbulent magnetic fluctuations spectrum in the proton gyroresonance frequency band with similar conclusion for He^{++} ions. The proton and He^{++} global parameters (such at temperatures, anisotropies, velocities, and drifts), the magnetic fluctuations spectra, and the ion velocity distributions close to the Sun modeled here can be directly compared to observations in future solar missions, such as Solar Orbiter and Solar Probe Plus.

Acknowledgments

The authors would like to acknowledge support by NASA grant NNX10AC56G.

Yuming Wang thanks the reviewers for their assistance in evaluating this paper.

References

Alexandrova, O., C. H. K. Chen, L. Sorriso-Valvo, T. S. Horbury, and S. D. Bale (2013), Solar wind turbulence and the role of ion instabilities, *Space Sci. Rev.*, *178*(2–4), 101–139, doi:10.1007/s11214-013-0004-8.

Araneda, J. A., A. F. Viñas, and H. F. Astudillo (2002), Proton core temperature effects on the relative drift and anisotropy evolution of the ion beam instability in the fast solar wind, *J. Geophys. Res.*, *107*(A12), 1453, doi:10.1029/2002JA009337.

Araneda, J. A., Y. Maneva, and E. Marsch (2009), Preferential heating and acceleration of α particles by Alfvén-cyclotron waves, *Phys. Rev. Lett.*, *102*(17), 175001, doi:10.1103/PhysRevLett.102.175001.

Axford, W. I., and J. F. McKenzie (1992), The origin of high speed solar wind streams, in *Solar Wind Seven Colloquium*, pp. 1–5, Pergamon Press, Oxford, U. K.

Bale, S. D., J. C. Kasper, G. G. Howes, E. Quataert, C. Salem, and D. Sundkvist (2009), Magnetic fluctuation power near proton temperature anisotropy instability thresholds in the solar wind, *Phys. Rev. Lett.*, *103*(21), 211101, doi:10.1103/PhysRevLett.103.211101.

Bourouaine, S., D. Verscharen, B. D. G. Chandran, B. A. Maruca, and J. C. Kasper (2013), Limits on alpha particle temperature anisotropy and differential flow from kinetic instabilities: Solar wind observations, *Astrophys. J.*, *777*, L3, doi:10.1088/2041-8205/777/1/L3.

Bruno, R., and V. Carbone (2005), The solar wind as a turbulence laboratory, *Living Rev. Sol. Phys.*, *2*(4), 1–187, doi:10.12942/lrsp-2005-4.

Case, A. W., et al. (2013), Designing a Sun-pointing Faraday cup for solar probe plus, in *American Institute of Physics Conference Series, American Institute of Physics Conference Series*, vol. 1539, edited by G. P. Zank et al., pp. 458–461, AIP Publishing LLC, Melville, N. Y., doi:10.1063/1.4811083.

Chandran, B. D. G., P. Pongkitiwanichakul, P. A. Isenberg, M. A. Lee, S. A. Markovskii, J. V. Hollweg, and B. J. Vasquez (2010), Resonant interactions between protons and oblique Alfvén/ion-cyclotron waves in the solar corona and solar flares, *Astrophys. J.*, *722*, 710–720, doi:10.1088/0004-637X/722/1/710.

Coleman, P. J. J. (1968), Turbulence, viscosity, and dissipation in the solar-wind plasma, *Astrophys. J.*, *153*, 371, doi:10.1086/149674.
Cranmer, S. R. (2000), Ion cyclotron wave dissipation in the solar corona: The summed effect of more than 2000 ion species, *Astrophys. J.*, *532*, 1197–1208.
Cranmer, S. R., G. B. Field, and J. L. Kohl (1999), Spectroscopic constraints on models of ion cyclotron resonance heating in the polar solar corona and high-speed solar wind, *Astrophys. J.*, *518*, 937–947.
Davidson, R. C., and J. M. Ogden (1975), Electromagnetic ion cyclotron instability driven by ion energy anisotropy in high-beta plasmas, *Phys. Fluids*, *18*, 1045–1050.
De Pontieu, B., et al. (2007), Chromospheric Alfvénic waves strong enough to power the solar wind, *Science*, *318*, 1574–1577, doi:10.1126/science.1151747.
Feldman, W. C., B. L. Barraclough, J. L. Phillips, and Y.-M. Wang (1996), Constraints on high-speed solar wind structure near its coronal base: A ULYSSES perspective, *Astron. Astrophys.*, *316*, 355–367.
Gary, S. P. (1993), *Theory of Space Plasma Microinstabilities*, Cambridge Univ. Press, New York.
Gary, S. P., L. Yin, D. Winske, and L. Ofman (2001), Electromagnetic heavy ion cyclotron instability: Anisotropy constraint in the solar corona, *J. Geophys. Res.*, *106*, 10,715–10,722, doi:10.1029/2000JA000406.
Gary, S. P., L. Yin, D. Winske, L. Ofman, B. E. Goldstein, and M. Neugebauer (2003), Consequences of proton and alpha anisotropies in the solar wind: Hybrid simulations, *J. Geophys. Res.*, *108*(A2), 1068, doi:10.1029/2002JA009654.
Gary, S. P., L. Yin, and D. Winske (2006), Alfvén-cyclotron scattering of solar wind ions: Hybrid simulations, *J. Geophys. Res.*, *111*, A06105, doi:10.1029/2005JA011552.
Gazis, P. R., and A. J. Lazarus (1982), Voyager observations of solar wind proton temperature—1–10 AU, *Geophys. Res. Lett.*, *9*, 431–434.
Gershman, D. J., T. H. Zurbuchen, L. A. Fisk, J. A. Gilbert, J. M. Raines, B. J. Anderson, C. W. Smith, H. Korth, and S. C. Solomon (2012), Solar wind alpha particles and heavy ions in the inner heliosphere observed with MESSENGER, *J. Geophys. Res.*, *117*, A00M02, doi:10.1029/2012JA017829.
Goldstein, B. E., E. J. Smith, A. Balogh, T. S. Horbury, M. L. Goldstein, and D. A. Roberts (1995), Properties of magnetohydrodynamic turbulence in the solar wind as observed by Ulysses at high heliographic latitudes, *Geophys. Res. Lett.*, *22*, 3393–3396.
Goldstein, B. E., M. Neugebauer, L. D. Zhang, and S. P. Gary (2000), Observed constraint on proton-proton relative velocities in the solar wind, *Geophys. Res. Lett.*, *27*, 53–56, doi:10.1029/1999GL003637.
Grappin, R., and M. Velli (1996), Waves and streams in the expanding solar wind, *J. Geophys. Res.*, *101*, 425–444, doi:10.1029/95JA02147.
Guhathakurta, M., A. Fludra, S. E. Gibson, D. Biesecker, and R. Fisher (1999), Physical properties of a coronal hole from a coronal diagnostic spectrometer, Mauna Loa Coronagraph, and LASCO observations during the Whole Sun Month, *J. Geophys. Res.*, *104*, 9801–9808, doi:10.1029/1998JA900082.
Hahn, M., and D. W. Savin (2013), Observational quantification of the energy dissipated by Alfvén waves in a polar coronal hole: Evidence that waves drive the fast solar wind, *Astrophys. J.*, *776*, 78, doi:10.1088/0004-637X/776/2/78.
Hellinger, P., and P. Trávníček (2006), Parallel and oblique proton fire hose instabilities in the presence of alpha/proton drift: Hybrid simulations, *J. Geophys. Res.*, *111*, A01107, doi:10.1029/2005JA011318.
Hellinger, P., and P. M. Trávníček (2011), Proton core-beam system in the expanding solar wind: Hybrid simulations, *J. Geophys. Res.*, *116*, A11101, doi:10.1029/2011JA016940.
Hellinger, P., and P. M. Trávníček (2013), Protons and alpha particles in the expanding solar wind: Hybrid simulations, *J. Geophys. Res. Space Physics*, *118*, 5421–5430, doi:10.1002/jgra.50540.
Hellinger, P., P. Trávníček, A. Mangeney, and R. Grappin (2003), Hybrid simulations of the expanding solar wind: Temperatures and drift velocities, *Geophys. Res. Lett.*, *30*(5), 1211, doi:10.1029/2002GL016409.
Hellinger, P., M. Velli, P. Trávníček, S. P. Gary, B. E. Goldstein, and P. C. Liewer (2005), Alfvén wave heating of heavy ions in the expanding solar wind: Hybrid simulations, *J. Geophys. Res.*, *110*, A12109, doi:10.1029/2005JA011244.
Hellinger, P., P. M. TráVníček, Š. Štverák, L. Matteini, and M. Velli (2013), Proton thermal energetics in the solar wind: Helios reloaded, *J. Geophys. Res. Space Physics*, *118*, 1351–1365, doi:10.1002/jgra.50107.
Hollweg, J. V. (2000), Cyclotron resonance in coronal holes: 3. A five-beam turbulence-driven model, *J. Geophys. Res.*, *105*, 15,699–15,714, doi:10.1029/1999JA000449.
Hollweg, J. V., and P. A. Isenberg (2002), Generation of the fast solar wind: A review with emphasis on the resonant cyclotron interaction, *J. Geophys. Res.*, *107*(A7), 1147, doi:10.1029/2001JA000270.
Hu, Y. Q., R. Esser, and S. R. Habbal (2000), A four-fluid turbulence-driven solar wind model for preferential acceleration and heating of heavy ions, *J. Geophys. Res.*, *105*, 5093–5112, doi:10.1029/1999JA900430.
Isenberg, P. A. (2004), The kinetic shell model of coronal heating and acceleration by ion cyclotron waves: 3. The proton halo and dispersive waves, *J. Geophys. Res.*, *109*, A03101, doi:10.1029/2002JA009449.
Isenberg, P. A., and B. J. Vasquez (2011), A kinetic model of solar wind generation by oblique ion-cyclotron waves, *Astrophys. J.*, *731*, 88, doi:10.1088/0004-637X/731/2/88.
Kaghashvili, E. K., B. J. Vasquez, and J. V. Hollweg (2003), Deceleration of streaming alpha particles interacting with waves and imbedded rotational discontinuities, *J. Geophys. Res.*, *108*(A1), 1036, doi:10.1029/2002JA009623.
Kasper, J. C., B. A. Maruca, M. L. Stevens, and A. Zaslavsky (2013), Sensitive test for ion-cyclotron resonant heating in the solar wind, *Phys. Rev. Lett.*, *110*(9), 091102, doi:10.1103/PhysRevLett.110.091102.
Kohl, J. L., et al. (1997), First results from the SOHO Ultraviolet Coronagraph Spectrometer, *Sol. Phys.*, *175*, 613–644.
Li, X., and S. R. Habbal (2005), Hybrid simulation of ion cyclotron resonance in the solar wind: Evolution of velocity distribution functions, *J. Geophys. Res.*, *110*, A10109, doi:10.1029/2005JA011030.
Li, X., S. R. Habbal, J. V. Hollweg, and R. Esser (1999), Heating and cooling of protons by turbulence-driven ion cyclotron waves in the fast solar wind, *J. Geophys. Res.*, *104*, 2521–2536, doi:10.1029/1998JA900126.
Liewer, P. C., M. Velli, and B. E. Goldstein (2001), Alfvén wave propagation and ion cyclotron interactions in the expanding solar wind: One-dimensional hybrid simulations, *J. Geophys. Res.*, *106*, 29,261–29,282, doi:10.1029/2001JA000086.
Lu, Q.-M., and S. Wang (2005), Proton and He^{2+} temperature anisotropies in the solar wind driven by ion cyclotron waves, *Chin. J. Astron. Astrophys.*, *5*, 184–192, doi:10.1088/1009-9271/5/2/009.
Maneva, Y. G., A. F. ViñAs, and L. Ofman (2013), Turbulent heating and acceleration of He^{++} ions by spectra of Alfvén-cyclotron waves in the expanding solar wind: 1.5-D hybrid simulations, *J. Geophys. Res. Space Physics*, *118*, 2842–2853, doi:10.1002/jgra.50363.
Maneva, Y. G., J. A. Araneda, and E. Marsch (2014), Regulation of ion drifts and anisotropies by parametrically unstable finite-amplitude Alfvén-cyclotron waves in the fast solar wind, *Astrophys. J.*, *783*, 139.
Marsch, E. (1991), Kinetic physics of the solar wind plasma, in *Physics of the Inner Heliosphere II. Particles, Waves and Turbulence, XI, 352 pp. 152 figs.*, pp. 45–133, Springer-Verlag, Berlin Heidelberg New York. Also Physics and Chemistry in Space, volume 21; 2.

Marsch, E. (1992), On the possible role of plasma waves in the heating of chromosphere and corona, in *Solar Wind Seven Colloquium*, edited by E. Marsch and R. Schwenn, pp. 65–68, Pergamon Press, Oxford, U. K.

Marsch, E., H. Rosenbauer, R. Schwenn, K. Muehlhaeuser, and F. M. Neubauer (1982a), Solar wind helium ions—Observations of the HELIOS solar probes between 0.3 and 1 AU, *J. Geophys. Res.*, *87*, 35–51, doi:10.1029/JA087iA01p00035.

Marsch, E., R. Schwenn, H. Rosenbauer, K.-H. Muehlhaeuser, W. Pilipp, and F. M. Neubauer (1982b), Solar wind protons—Three-dimensional velocity distributions and derived plasma parameters measured between 0.3 and 1 AU, *J. Geophys. Res.*, *87*, 52–72.

Maruca, B. A., J. C. Kasper, and S. D. Bale (2011), What are the relative roles of heating and cooling in generating solar wind temperature anisotropies? *Phys. Rev. Lett.*, *107*(20), 201101, doi:10.1103/PhysRevLett.107.201101.

Matteini, L., P. Hellinger, B. E. Goldstein, S. Landi, M. Velli, and M. Neugebauer (2013), Signatures of kinetic instabilities in the solar wind, *J. Geophys. Res. Space Physics*, *118*, 2771–2782, doi:10.1002/jgra.50320.

McComas, D. J., et al. (2007), Understanding coronal heating and solar wind acceleration: Case for in situ near-Sun measurements, *Rev. Geophys.*, *45*, RG1004, doi:10.1029/2006RG000195.

McComas, D. J., et al. (2008), Solar probe plus: Report of the Science and Technology Definition Team (STDT), *NASA/TM-2008-214161*.

Neugebauer, M., B. E. Goldstein, E. J. Smith, and W. C. Feldman (1996), Ulysses observations of differential alpha-proton streaming in the solar wind, *J. Geophys. Res.*, *101*, 17,047–17,056, doi:10.1029/96JA01406.

Ofman, L. (2010a), Hybrid model of inhomogeneous solar wind plasma heating by Alfvén wave spectrum: Parametric studies, *J. Geophys. Res.*, *115*, A04108, doi:10.1029/2009JA015094.

Ofman, L. (2010b), Wave modeling of the solar wind, *Living Rev. Sol. Phys.*, *7*, 4.

Ofman, L., and A. F. Viñas (2007), Two-dimensional hybrid model of wave and beam heating of multi-ion solar wind plasma, *J. Geophys. Res.*, *112*, A06104, doi:10.1029/2006JA012187.

Ofman, L., A. Viñas, and S. P. Gary (2001), Constraints on the O^{+5} anisotropy in the solar corona, *Astrophys. J.*, *547*, L175–L178, doi:10.1086/318900.

Ofman, L., S. P. Gary, and A. Viñas (2002), Resonant heating and acceleration of ions in coronal holes driven by cyclotron resonant spectra, *J. Geophys. Res.*, *107*(A12), 1461, doi:10.1029/2002JA009432.

Ofman, L., J. M. Davila, V. M. Nakariakov, and A.-F. Viñas (2005), High-frequency Alfvén waves in multi-ion coronal plasma: Observational implications, *J. Geophys. Res.*, *110*, A09102, doi:10.1029/2004JA010969.

Ofman, L., A.-F. Viñas, and P. S. Moya (2011), Hybrid models of solar wind plasma heating, *Ann. Geophys.*, *29*, 1071–1079, doi:10.5194/angeo-29-1071-2011.

Omidi, N., P. Isenberg, C. T. Russell, L. K. Jian, and H. Y. Wei (2014), Generation of ion cyclotron waves in the corona and solar wind, *J. Geophys. Res. Space Physics*, *119*, 1442–1454, doi:10.1002/2013JA019474.

Podesta, J. J., D. A. Roberts, and M. L. Goldstein (2006), Power spectrum of small-scale turbulent velocity fluctuations in the solar wind, *J. Geophys. Res.*, *111*, A10109, doi:10.1029/2006JA011834.

Raymond, J. C., et al. (1997), Composition of coronal streamers from the SOHO Ultraviolet Coronagraph Spectrometer, *Sol. Phys.*, *175*, 645–665.

Smith, C. W., B. J. Vasquez, and K. Hamilton (2006), Interplanetary magnetic fluctuation anisotropy in the inertial range, *J. Geophys. Res.*, *111*, A09111, doi:10.1029/2006JA011651.

Stix, T. H. (1962), *The Theory of Plasma Waves*, McGraw-Hill, New York.

Tomczyk, S., and S. W. McIntosh (2009), Time-distance seismology of the solar corona with CoMP, *Astrophys. J.*, *697*, 1384–1391, doi:10.1088/0004-637X/697/2/1384.

Tu, C.-Y., and E. Marsch (1997), Two-fluid model for heating of the solar corona and acceleration of the solar wind by high-frequency Alfven waves, *Sol. Phys.*, *171*, 363–391.

Vasquez, B. J., C. W. Smith, K. Hamilton, B. T. MacBride, and R. J. Leamon (2007), Evaluation of the turbulent energy cascade rates from the upper inertial range in the solar wind at 1 AU, *J. Geophys. Res.*, *112*, A07101, doi:10.1029/2007JA012305.

Wambecq, A. (1978), Rational Runge-Kutta methods for solving systems of ordinary differential equations, *Computing*, *20*, 333–342.

Winske, D., and N. Omidi (1993), *Computer Space Plasma Physics: Simulation Techniques and Software,* edited by H. Matsumoto and Y. Omura, pp. 103–160.

Xie, H., L. Ofman, and A. Viñas (2004), Multiple ions resonant heating and acceleration by Alfvén/cyclotron fluctuations in the corona and the solar wind, *J. Geophys. Res.*, *109*, A08103, doi:10.1029/2004JA010501.